Available online at www.sciencedirect.com

SciVerse ScienceDirect

Scripta Materialia 68 (2013) 945–948

Scripta MATERIALIA

www.elsevier.com/locate/scriptamat

Interrupted ageing in steels: Hardness improvement and microstructural stabilization

B. Kim,[a] C. Celada,[b] D. San Martín,[b] J. Chao,[b] J. Vara[b] and P.E.J. Rivera-Díaz-del-Castillo[a,*]

[a] *Department of Materials Science and Metallurgy, University of Cambridge, Pembroke Street, Cambridge CB2 3QZ, UK*
[b] *MATERALIA Group, Department of Physical Metallurgy, Centro Nacional de Investigaciones Metalúrgicas (CENIM-CSIC), Av. Gregorio del Amo 8, 28040 Madrid, Spain*

Received 6 February 2013; revised 12 February 2013; accepted 16 February 2013
Available online 27 February 2013

Similarly to aluminium alloys, interrupted ageing in steels may increase hardness by 10%. By adding an intermediate stage between quenching and tempering, where quenched martensite is left to age at room temperature, carbon forms finer precipitate microstructures, which become more stable at room temperature. Using thermoelectric power to model carbon segregation to dislocations, it appears that room temperature ageing increases the number of effective nucleation sites for the subsequent tempering stage, as reflected in the microstructure and hardness.

Keywords: Ageing; Martensitic steels; Interstitial diffusion; Hardness; Carbides

In freshly quenched martensite, where the diffusion of solutes is restricted because of slow kinetics at room temperature, only interstitials such as carbon and nitrogen diffuse significantly. The distribution of carbon atoms immediately after quenching has a marked effect on the subsequent heat treatment [1]. It is understood that in freshly quenched martensite, carbon becomes trapped by defects, such as dislocations, as these display a strain field to which solutes such as carbon become attracted. Carbon atoms gather in the vicinity of the dislocation forming the so-called Cottrell atmospheres, cancelling the dislocation strain, resulting in a pinning effect [2]. The present work introduces an intermediate stage between quenching and tempering, called interrupted ageing (IA). During this stage, the freshly quenched martensite is left to age at room temperature, allowing for controlled carbon segregation into dislocations, resulting in increased hardness and more stable precipitate structures.

A technique that has been employed in order to study carbon-controlled reactions, such as precipitation, is thermoelectric power (TEP) [3–8]. The main benefit of TEP is attributed to its sensitivity in detecting atoms in solid solution, which can be exploited for tracking the kinetics of carbon diffusion during IA. TEP measurements, combined with the model originally devised by Kalish and Cohen [1], provide further understanding of the interrelationship between processing, microstructure and the mechanical properties of mid-carbon steels undergoing IA.

An automotive industrial grade of composition Fe–0.55C–1.6Si–0.7Mn–0.5Cr–0.13V (wt.%), where Cu, Ni and Mo were present as tramp elements, was used in this study. The as-received material was in the form of rods, with an initial hardness of 317 HV1. The specimens were heat treated in an Adamel Lhomargy dilatometer (model DT1000) in order to study interruption, tempering time and temperature. The specimens were cylindrical rods 3 mm in diameter and 12 mm in length. The heat treatment was carried out as shown in Table 1.

T_1 and t_1 are the austenitization temperature and time, respectively; T_2 and t_2 are the tempering temperature and time, respectively; and t_{IA} is the duration of the room temperature interruption. For all conditions, the samples were heated at a rate of 10 °C s^{-1}, austenitized for 180 s, quenched to 55 °C using helium flux at 300–500 °C s^{-1}, held for 60 s and then allowed to cool down to room temperature. The samples undergoing IA were removed from the dilatometer and left to age at room temperature before the subsequent tempering stage.

* Corresponding author. Tel.: +44 (0) 1223334300; e-mail: pejr2@cam.ac.uk

1359-6462/$ - see front matter © 2013 Acta Materialia Inc. Published by Elsevier Ltd. All rights reserved.
http://dx.doi.org/10.1016/j.scriptamat.2013.02.036

Table 1. Heat treatment summary for the nine conditions investigated.

	T_1 (°C)	t_1 (s)	t_{IA}	T_2 (°C)	t_2 (s)
L1	880	180	7.2 h	250	1800
L2	880	180	3 days	250	1800
L3	880	180	30 days	250	1800
L4	880	180	30 days	250	300
L5	880	180	–	–	–
L6	880	180	–	250	1800
L7	880	180	–	250	5400
L8	880	180	–	300	1800
L9	880	180	30 days	300	1800

The critical transformation temperatures were determined from dilatometry as $Ac_1 = 798 \pm 3$ °C and $Ac_3 = 832 \pm 3$ °C, $M_s = 238 \pm 9$ °C, where Ac_1 and Ac_3 are the austenitization start and finish temperature, and M_s is the start temperature. These are the average values of 10 different experiments. The prior austenite grain boundaries were revealed by the thermal etching method [9], and an average grain size of 5 ± 1 μm was estimated from light optical micrographs, using the mean linear intercept method [10].

After heat treatment, the samples were characterized using transmission electron microscopy (Philips CM30 model). Over 500 intralath precipitate particles were analysed per condition, taken from three to four different TEM frames, all under the same magnification, ×52k. The length, width and centre-to-centre particle spacing were measured. Having applied stereological corrections [11], the shape of the carbide was approximated to a cylinder, from which the equivalent radius of a sphere was extracted. This was carried out for comparison purposes only, as the aspect ratio varied slightly throughout the different conditions. Vickers hardness tests were carried out using a Mitutoyo MVK-H2 microhardness indenter with a 1 kg load.

Representative microstructures are shown in Figure 1a for conditions L3, L6, L8 and L9. Following detailed microstructural analysis, the particle size and spacing relationship are shown in Figure 1b. The general trend observed is that particle size decreases with increasing temperature, whereas particle spacing decreases with the interruption time.

As a way of ensuring that the microstructures of the two conditions were statistically distinct, Kolmogorov–Smirnov (K–S) statistical tests [12] were carried out (not presented in here). Given two precipitate size distributions, x_1 and x_2, the K–S test states the null hypothesis that x_1 and x_2 are from the same continuous distribution. The output of the test is either a 1 or a 0, where 1 rejects the null hypothesis, i.e., x_1 and x_2 are not from the same continuous distribution, and 0 infers a valid hypothesis. Based on Figure 1b and confirmed by the outcome from the K–S test, the observed trend was that IA results in a finer microstructure in terms of smaller particle size and spacing (L3 vs. L6 and L9 vs. L8), and that the duration of tempering (t_2) after 30 days of IA did not influence the microstructure (L3 vs. L4). Tempering at a higher temperature after IA led to smaller carbides, without altering their spacing (L3 vs. L9).

The IA stage leads to finer microstructures; it can be postulated that IA provides a more efficient take-up of

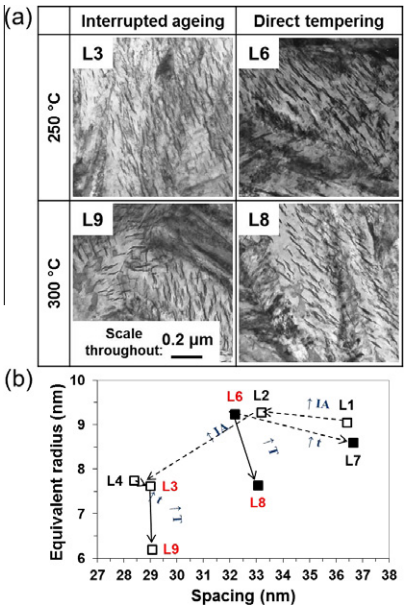

Figure 1. (a) Representative bright-field images shown for conditions L3, L6, L8 and L9, and (b) particle size and spacing represented on a grid, where the arrows labelled "t", "IA" and "T" indicate an increase in tempering time, interruption time and tempering temperature, respectively.

carbon atoms from the solid solution. During the time at room temperature, the carbon atoms are likely to diffuse into defect traps, such as dislocations. Allowing segregation into dislocations increases the number of effective nucleation sites for the tempering stage, evidenced in the finer microstructure obtained (L3 vs. L6 and L9 vs. L8).

Differences in hardness were observed for the same conditions over a period of 6 months (Figure 2). The percentage hardness variation for each condition is shown on top of the bars. The error bars represent one standard deviation. The biggest change during the 6 months is observed in L6, followed by L7. Since both were tempered at 250 °C, it follows that the tempering reaction does not come to completion at 250 °C, and so continues at room temperature at a slower pace, a phenomenon that has been reported in the literature [13]. This is further consistent with the fact that the change observed in L8 is less than that in L6, where L8 having been tempered at 300 °C would have reached a higher degree of reaction completion than L6, which was tempered at 250 °C.

Condition L9 shows distinctive behaviour: the introduction of IA increases hardness with respect to L8, but

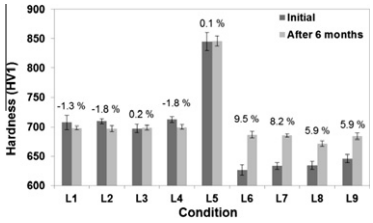

Figure 2. Hardness changes over 6 months.

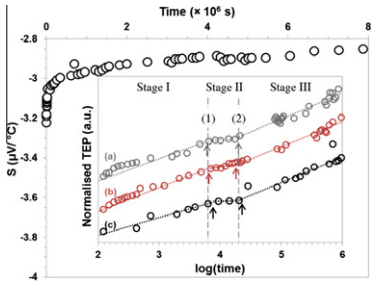

Figure 3. TEP evolution for the as-quenched state (shown for sample (c)), where the inset shows the three TEP runs in logarithmic scale. The arrows mark transition points detected in TEP.

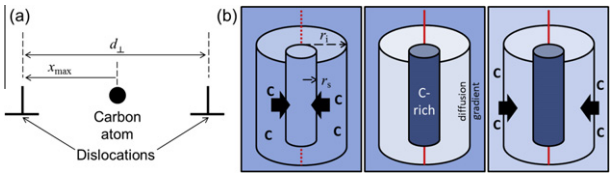

Figure 4. (a) Schematic diagram showing the planar view of a dislocation segment in relation to a carbon atom, and (b) summary of the carbon segregation to dislocation strain fields, after Ref. [1].

hardness is not stabilized at room temperature. Compared with L3, this may be due to a finer precipitate size; in fact, L9 displays the smallest carbide size, which would lead to a lesser degree of precipitation hardening if a shearing mechanism is assumed [14]. On further room temperature ageing, the particles may grow further, increasing hardness.

Complementary to the characterization work, TEP measurements were carried out on quenched specimens of dimensions $30 \times 2 \times 1$ mm, using a TechLab-GEMPPM INSA Lyon model. Its operation consists in clamping the two extremes of the rectangular plate on two metallic (copper for this work) reference blocks. These blocks are kept at 15 and 25 °C, thus, a temperature gradient ΔT of 10 °C is applied and a response in voltage ΔV is recorded. Schematic diagrams are shown in Ref. [4]. The TEP, S^*, of the tested material is given by

$$S = S^* - S^*_{Cu} = \frac{\Delta V}{\Delta T} \tag{1}$$

where S is the observed TEP, S^*_{Cu} is the TEP of the reference blocks (pure copper, 99.99 wt.%, $S^* = 1.91\ \mu V\ K^{-1}$, at 20 °C). The TEP evolution in the as-quenched state was recorded over a period of 3 months. Three runs were made for reproducibility (Figure 3).

As observed in Figure 3, the TEP signal increases with time, until it appears to approach a constant value. Shown on the inset, two transition points were observed, where the TEP appears to change. The separation into the three regions is discussed in the forthcoming section. It is established that the observed TEP is the result of various terms [15]:

$$S^* = S^*_0 + \Delta S_{ss} + \Delta S_d + \Delta S_{pcpt} \tag{2}$$

where S^*_0 is the TEP of the base metal, ΔS_{ss} is due to the elements in solid solution, ΔS_d is due to dislocations, and ΔS_{pcpt} is due to the presence of precipitates. Such observation has been related to the interaction of free carbon atoms in solid solution and dislocations in pre-strained ultra-low carbon steels [8]. During room temperature ageing of quenched martensite, carbon segregation into dislocation cores would cancel out the strain fields of the latter, hence the ΔS_d term would evolve. Similarly, the signal due to solid solution would also evolve, as less "free" carbon in solid solution remains. The ΔS_{pcpt} term becomes significant only in the case of small, coherent precipitates [6]. For the sake of simplicity, the following assumptions are made to interpret TEP evolution: (i) quenching is sufficiently fast to avoid small coherent carbide precipitation during cooling; (ii) the carbon–dislocation interaction energy remains constant until the dislocation core becomes saturated, i.e., ΔS_d remains constant during early segregation stages; (iii) then, in the first instances after quenching, the decrease in TEP magnitude is due to C segregation alone.

Consider a planar view of a dislocation segment (Fig. 4a). Assuming a uniform distribution of dislocations throughout the material, for a given dislocation density ρ, the average spacing between dislocations $d_\perp$ can be determined:

$$d_\perp = \frac{1}{\sqrt{\rho}} \tag{3}$$

A "free" carbon atom in solid solution is bound to be attracted to the vicinity of a dislocation due to the exerted strain field. One way of approximating the diffusing distance of these carbon atoms is to state that a carbon that is initially found in the middle between two parallel dislocations would need to travel a maximum distance x_{max} that is half the average spacing between dislocations, i.e., 0.5 $d_\perp$ (Fig. 4a). Given a suitable value for the diffusion coefficient of carbon in α-Fe, $D_{C,\alpha}$, the time t to complete segregation would be determined by x_{max}:

$$x_{max} \approx \sqrt{2 D_{C,\alpha} t} \tag{4}$$

Revisiting the original work of Kalish and Cohen [1], in the vicinity of a dislocation there are two areas of interest: the segregation zone r_s and the interaction zone r_i. The former is the immediate region that encloses the dislocation line, where carbon atoms segregate into at the first instance. Once all the solutes have been stored at the dislocation core, those carbon atoms from the latter region begin diffusing inwards, leaving behind a depleted region. Consequently, a diffusion gradient is established, thus drawing in further carbon from elsewhere in the matrix. The process is summarized in Figure 4b.

Beyond the limit of the interaction zone, i.e., r_i, a carbon atom no longer experiences any interaction energy with dislocations, and the energy is solely given by the thermal term kT, where k is the Boltzmann constant, and T is the absolute temperature. The interaction energy at the dislocation core has been stated to be 0.46 eV at a distance of one Burgers vector (1**b**) [1]. This means that, at the limit of r_i, a carbon atom has a thermal energy of $kT = 0.026$ eV, where $k = 8.62 \times$

Table 2. Characteristic time scale of martensite ageing at room temperature, where IE is the carbon–dislocation interaction energy.

	Time (h)	$<x>$ (nm)	IE (eV)
1	1.8 ± 0.2	1.9 (7.7**b**)	0.060
2	5.5 ± 0.6	3.3 (13.3**b**)	0.034

10^{-5} eV K^{-1} and $T = 298$ K, equivalent to a distance of 17.8**b**.

The transition points marked (1) and (2) on the inset on Figure 3 can be used to determine the process outlined in the Kalish–Cohen model, where the three regions appear to be:

- Stage I: initial segregation, where the nearest carbon (i.e., within r_s) diffuses into the core of the dislocation.
- Stage II: solute competition. Once r_i becomes depleted, adjacent dislocations (or existing carbides) compete for the remaining carbon in the matrix. Minimum carbon activity is seen overall, which could account for the decrease in slope.
- Stage III: diffusion into the depleted region.

Following the assumptions previously stated, given the times marked (1) and (2) in Figure 3, the corresponding diffusing distance of carbon atoms can be calculated using Eq. (4), where at 25 °C, $D_{C,\alpha} = 2.8 \times 10^{-22}$ m^2 s^{-1} [16]. The Kalish–Cohen model can be applied in order to determine the corresponding dislocation–carbon atom interaction energy (Table 2).

Dilatometry experiments showed that the M_s for this alloy was 238 ± 9 °C, which would correspond to a dislocation density of 8×10^{15} m^{-2} [11]. Hence, the average distance between trapping sites would then be $d_\perp = 11.2$ nm, so $x_{max} = 5.6$ nm. Then, since $<x>$ at point (2) is $<x_{max}$, this infers that, even after 5.5 h of room temperature ageing, "free" carbon still remains in solid solution. In addition, the fact that at the end of Stage II, the dislocation–carbon atom interaction energy is about 0.034 eV, which starts to approach the interaction limit $kT = 0.026$ eV, seems to support the idea that the transition from Stage II to Stage III is due to carbon depletion within the interaction zone.

Based on the TEP measurements, it appears that, within 2 h after quenching (end of Stage I), there is already some carbon segregating into dislocations. This is reflected in the higher hardness, even after 7 h of IA (condition L1), although the microstructural change is not so obvious. From the fact that the TEP signal changes even after 3 months, it can be inferred that there continues to be some carbon activity within the matrix although, by the slow flattening of the curve, the kinetics appear to have decreased. The continuous increase in the TEP signal implies an ongoing carbon segregation process even after 5.5 h of interruption time, possibly leading to a more homogeneous dispersion of carbon across the matrix prior to tempering. This explains the continuous refinement of the microstructure observed throughout L2 and L3.

To summarize, IA in mid-carbon steels may be employed to increase hardness (~10%), and to foster the stability of the precipitate structure. On quenching, the interruption allows for carbon migration towards dislocation cores, as pointed out by TEP measurements. Such uniform redistribution is consistent with the formation of nuclei whose spacing reduces with interruption time. The effective and efficient allocation of carbon in fine precipitates ensures that properties such as hardness become stabilized. This may be exploited in applications where dimensional stability and constant hardness are required throughout component life.

B.K. and P.E.J.R. are grateful to Prof. A.L. Greer for the provision of laboratory facilities, and acknowledge ASCOMETAL for financial support. DSM acknowledges financial support from Ministerio de Economía y Competitividad (Project No. MAT2010-19522).

[1] D. Kalish, M. Cohen, Mater. Sci. Eng. 6 (1970) 156.
[2] A.H. Cottrell, B.A. Bilby, Proc. Phys. Soc. A 62 (1949) 49.
[3] D. Benkirat, P. Merle, R. Borrelly, Acta Metall. 36 (1988) 613.
[4] M. Perez, C. Sidoroff, A. Vincent, C. Esnouf, Acta Mater. 57 (2009) 3170.
[5] F.G. Caballero, C. Capdevila, L.F. Alvarez, C. García de Andrés, Scripta Mater. 50 (2004) 1061.
[6] J.M. Pelletier, G. Vigier, J. Merlin, P. Merle, F. Fouquet, R. Borrelly, Acta Metall. 32 (1984) 1069.
[7] N. Lavaire, V. Massardier, J. Merlin, Scripta Mater. 50 (2004) 131.
[8] N. Lavaire, J. Merlin, V. Sardoy, Scripta Mater. 44 (2001) 553.
[9] D. San Martín, Y. Palizdar, R.C. Cochrane, R. Brydson, A.J. Scott, Mater. Charact. 61 (2010) 584.
[10] ASTM Standard E112-10, Standard Test Methods for Determining Average Grain Size, ASTM International, West Conshohocken, PA, http://dx.doi.org/10.1520/E0112-10, Available from: <www.astm.org>.
[11] C.H. Young, H.K.D.H. Bhadeshia, Mater. Sci. Technol. 10 (1994) 209.
[12] MathWorks, Two-sample Kolmogorov-Smirnov test http://www.mathworks.co.uk/help/stats/kstest2.html.
[13] B.L. Averbach, M. Cohen, S.G. Fletcher, Trans. ASM 40 (1948) 728.
[14] T. Gladman, Mater. Sci. Technol. 15 (1999) 30.
[15] S. Carabajar, J. Merlin, V. Massardier, S. Chabanet, Mater. Sci. Eng. A 281 (2000) 132.
[16] R.P. Smith, Trans. AIME 224 (1962) 105.